Structure of refrozen cracks in first–year sea ice

Chris Petrich, Tim G. Haskell, and Pat J. Langhorne

Abstract: The structure of natural refrozen cracks in landfast first–year sea ice in McMurdo Sound, Antarctica, is examined in spring. Alignment of inclusions, crystal profile and two–dimensional salinity profile are discussed and compared to freezing experiments of slots cut in sea ice sheets. Convection in the water column during the phase transition is modelled with the Finite Volume Method. The investigated cracks and slots are to the order of 20 to 30 cm wide and grown in ice of about 1 to 2.2 m thickness. We find that inclusions seem to align with the freezing front, and suggest that crystal structure and salinity profile are influenced by naturally driven convection inside refreezing cracks.

1. Introduction

In the investigation of natural sea ice most effort has focused on sea ice that has frozen with heat flow in predominantly one dimension [1]. Leads and cracks provide the opportunity to study sea ice growth under two–dimensional heat flow, i.e. heat flow to the ocean–air interface and to the surrounding sea ice. In this paper, we pinpoint some characteristic morphological features that are relevant to the growth processes of sea ice.

Sea ice grows from a solution of salts in water. Although the solutability of ions in ice is generally low, the overall salinity of sea ice is still 10 to 50 % that of seawater [1,2] because brine is entrapped in the growing ice matrix [1,3,4]. This brine is subject to removal processes described by Untersteiner [5], of which brine expulsion due to gravity drainage is the most important to sea ice desalination [1]. Common desalination features are brine drainage channels or tubes, and networks [6–9]. Although they have been investigated in the field [3, 8], their evolutionary processes have mostly been the target of theoretical work (e.g. [10–13]) and laboratory experiments (e.g. [14–19]). When we deal with brine inclusions in refrozen cracks in this paper, we will demonstrate the correspondence between inclusion alignment and the orientation of the freezing front.

We also consider the crystal orientations in refrozen cracks. Depending on the growth history of the host sea ice, crystal size, shape, and alignment are known to vary considerably [1]. The prevalent columnar ice crystals are elongated vertically, as described by Weeks and Ackley [1], due to geometric selection. As we will see in refrozen cracks, the long crystals away from the center are rather horizontally elongated than vertically. We suggest that their orientation is due to a combination of geometrical selection and a vertical salinity gradient at the freezing interface.

In section 2 we present structural observations of two natural refrozen cracks on landfast first–year

C. Petrich and P.J. Langhorne.[1] University of Otago, Physics Department, P.O. Box 56, Dunedin, New Zealand
T.G. Haskell. Industrial Research Ltd., P.O. Box 31-310, Lower Hutt, New Zealand

[1] Corresponding author: (e-mail: pjl@physics.otago.ac.nz).

 © NRC Canada

Fig. 1. a) Vertical salinity profile showing sampled sections and b) contoured vertical salinity profile of natural crack *nc1*. Salinities are given in psu. The hoizontal center of the crack is at 0 mm, and the host ice starts at $\pm$150 mm. The outermost boxes of the salinity profile in a) are the host sea ice. c) Vertical thick section of natural crack *nc1*.

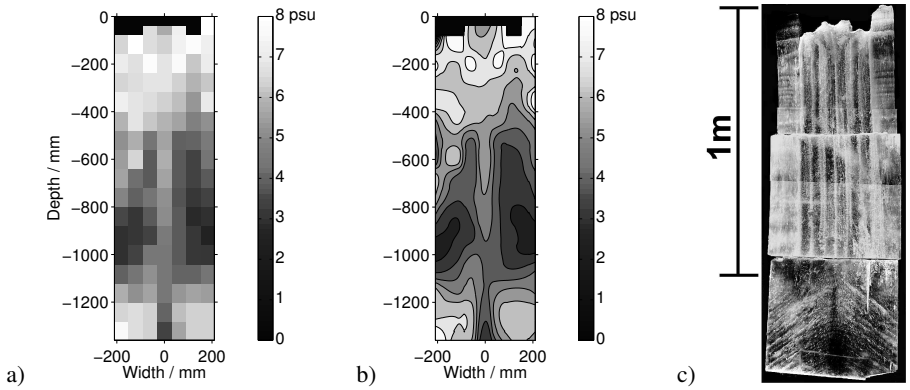

sea ice in McMurdo Sound, Antarctica, sampled in October and November 2001. Since these cracks froze in conditions unknown to us, we performed controlled refreezing experiments by cutting a slot through the ice sheet. The salinity and crystallography of this refrozen material is presented in section 3. In an attempt to determine the relevant parameters governing ice growth we develop a model based on the Finite Volume Method (FVM). Results relevant to the refreezing of cracks are described in section 4. In section 5 we summarize our findings, and draw conclusions and implications for future work.

2. Natural Cracks

We have examined various natural cracks that apparently refroze in a divergent regime, i.e. they are not rafted. A surface indication of their structural difference to the host ice sheet is the observation that even refrozen "cracks" 10 meters wide do not exhibit star–like brine structures found on the adjacent sea ice sheet. However, structural differences between the host sea ice and cracks are found to continue deeper into the ice. In this study we focus on rather small refrozen cracks, about 20 to 30 cm wide, that exhibited a freeboard of roughly 10 cm. Two cracks are examined in detail here.

2.1. nc1

Crack *nc1* (see Fig. 1) has a step profile at the ice–air interface with an overall width of 24 cm and a freeboard of 8 cm, indicating that refreezing began at an ice thickness of about 1 m. At the time of examination in October the surrounding bulk ice was 2.2 m deep. A specially equipped digger [20] was used to cut out a 140 cm deep profile of this crack, that was then sectioned into blocks $6 \times 8 \times 10$ cm^3, and melted to determine the salinity with a conductivity probe. The salinity profile in Figs. 1a and b exhibits various interesting features: first, we notice the high degree of symmetry in this work of nature. Further, the crack itself seems to exhibit a collar of high salinity in the top 200 mm, and from 400 to 1000 mm we find a center line of high salinity with respect to the immediate neighborhood. From 1000 mm downwards, however, the center is less saline than the surrounding. The transition from crack ice to host ice does not produce a sharp discontinuity in the salinity profile.

The transition at 1000 mm coincides with a structural change of the inclusions seen in the thick section of Fig. 1c. With the exception of the top 200 mm with its V–shaped divergence, the upper 1000 mm are marked by seven vertical bands of inclusions, the outermost pair presumably following

© NRC Canada

Fig. 2. a) Vertical salinity profile showing sampled sections and b) contoured vertical salinity profile of natural crack *nc5*. The entire salinity profile is in the crack. The salinity profile is mirrored about width = 0 mm. c) Vertical thick section of natural crack *nc5*.

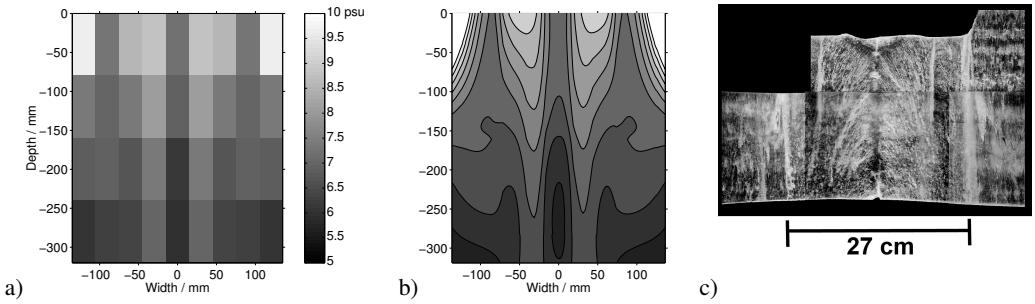

the crack edges. The inclusions of the bottom 400 mm follow lines of about 60° from the vertical and are arch shaped near the center. The center of this bottom section is free of inclusions visible to the naked eye. Thin sections not shown in this paper reveal a frazil–like crystal array in the upper 1000 mm, and columnar crystals in the bottom section investigated.

We suggest that this crack formed as a series of fracture events that took place when the bulk ice has reached a thickness of 1 m. Tension may have build up in the ice sheet that has suddenly been released at the crack [21]. The crack has refrozen and tension has build up again to be released by another breaking event. There could have been three fracture events with the vertical lines of inclusions marking the sides and the center of the crack where brine has been expelled ahead of the freezing interface. The cracks may have been too narrow for fluid motion to occur, particularly if dendrites have grown out from the face of the crack. The hypothesis of multiple fracture events is further supported by the observation that this crack has branched off and reunited several times over a kilometer.

2.2. nc5

Crack *nc5* (Fig. 2) has a smooth surface at the ice–air interface with an overall width of 27 cm and a freeboard of 8.5 cm. The topmost 40 cm of this crack were cut out with a chain saw, sectioned into blocks $3 \times 8 \times 10$ cm^3, and the salinity was measured as in the case of *nc1*. All of the blocks of the salinity profile in Fig. 2a are from crack ice itself, and the rightmost four columns are mirror images of the leftmost four columns. The salinity profile shows a region of low salinity along the crack's center with a band of high salinity adjacent. This profile resembles the region deeper than 1000 mm of Fig. 1c rather than the top 1000 mm of *nc1*.

In the vertical thick section of Fig. 2c we notice ± 85 mm from the center, two 125 mm long vertical bands of inclusions at the surface that frame a region of arch shaped inclusions. The arches are steeper than the ones of *nc1*. The center is relatively free of inclusions, and a rather transparent V–shaped structure again appears at the ice-air interface. We could imagine that this crack, too, used to be narrower, refroze at the top to break up again and refreeze completely.

Fig. 3 displays a composite image of vertical thin sections across the crack. The difference in crystal structure between host ice and crack ice is obvious. While the crystals in the host form a vertical pattern characteristic of columnar ice, the crack crystals form a roughly horizontal pattern with the exception of the center region. The center region is marked by vertically aligned crystals with their c-axes parallel to the crack axis. Towards the top it branches off into a V-shaped pattern corresponding to the transparent V-shape observed in the thick section. An interesting feature of the crystal structure we have noticed repeatedly is that the long axis of the crystals at the sides is tilted to the horizontal. We may attempt an explanation in the following way. At the freezing front of every excavated slot (see next

© NRC Canada

Fig. 3. Vertical thin section of natural crack *nc5*.

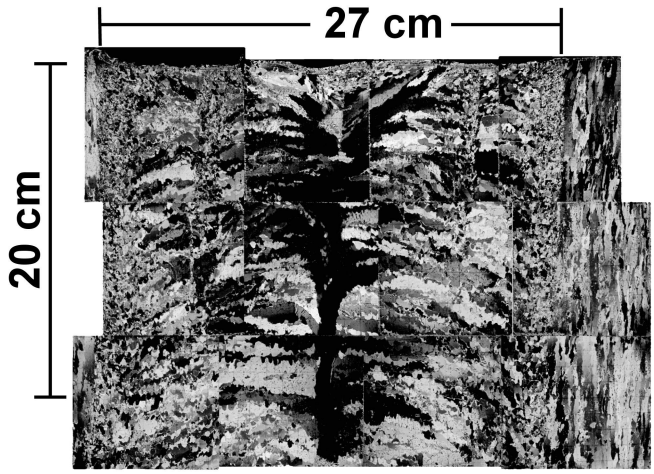

section) and at the ice–water interface of every excavated host ice sample we found oriented cm–size platelets. As observed, they grew vertically inside the slots, i.e. with their c–axes parallel to the crack, presumably because this orientation grows most rapidly. During the growth of the majority of ice, we expect convective currents in the crack with upwelling fresh seawater in the center and downwelling brine at the sides. Assuming that the salinity of the brine increases with depth in the downwelling stream there could be an incentive for the crystals to grow towards the less saline region that would be closer to the top.

Contrary to observations in bulk ice, where brine channels intersect the ice–water interface at approximately 90°, brine channels are aligned as arches in this thick section. We suppose the inclusions did not migrate there from the vertical but instead simply formed there during freezing, trapped between newly growing crystals. They therefore mark the freezing front of the crack. However, this does not preclude they may have moved somewhat due to a thermal gradient or pressure induced micro–crack migration [5].

The low salinity in the crack's center again corresponds to a relatively low number of inclusions in this area. A slightly higher salinity has been measured at adjacent locations, where we find the arches. We suggest that upwelling fresh seawater efficiently removes inclusions from the freezing front of the crystals at the center. Since the upwelling current should split to form a V–shaped pattern at the top of the crack, we attribute the low number of inclusions in that area to the flow of relatively low salinity seawater as well.

3. Artificial Cracks or Slots

We have conducted two–dimensional freezing experiments in the field to take various measurements. Of these, we discuss in this paper the salinity profile, the inclusion structure, and the crystal alignment. Slots 20 to 30 cm wide were cut through 1.3 to 2.2 m thick first–year ice with the digger. After about one week of refreezing ice at the top of the arch is 40 cm thick, and samples were cut.

The salinity profile of the 240 mm wide slot, *slot1*, shown in Figs. 4a and b is of crack ice, only. We see two leg–like structures of higher salinity surrounding the low salinity center. There was a big inclusion at the center of the crack, about 60 mm below the crack surface, 60 mm wide and 10 mm deep. We think it is an air inclusion that either drifted into the crack from under the host ice, or the result of a failed attempt to breathe by a local seal. Such inclusions seem to occur frequently. The

© NRC Canada

Fig. 4. a) Vertical salinity profile showing sampled sections and b) contoured vertical salinity profile of slot *slot1*. The entrire salinity profile is in the crack. c) Vertical thick section and d) vertical thin section of *slot2* 230 mm below the slot surface. Indicated is the slot width of 32 cm.

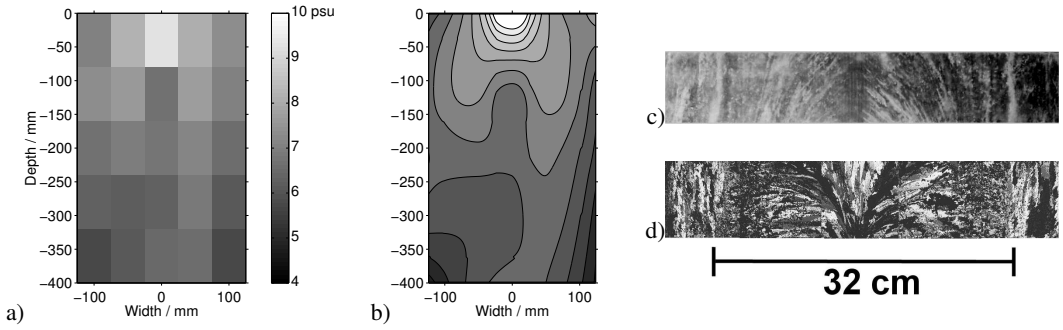

salinity profile is symmetric, and a similarity to the salinity profile of *nc5* is apparent. We are led to the belief that this is yet another example of increased salinity in the vicinity of brine channels as recently reported by Cottier et al. [9].

Figs. 4c and d compare thick section and thin section, respectively of 32 cm wide slot *slot2*. The 80 mm high sections, 230 to 310 mm below the slot's surface, show the typical arched shaped brine structures and the corresponding crystal alignment. Interestingly, unlike the examples of natural cracks, the vertical crystals in the center generally do not have their c–axes aligned along the length of the crack. Also, the crystals seem smaller. In the thin section of Fig. 4d the crystals close to the boundary do not point upwards into the center as observed in the natural cracks and other slot experiments.

4. Numerical Model Calculations

We perform a two–dimensional numerical simulation of ice growth in cracks using the Finite Volume Method (FVM) [22, 23], with the enthalpy–porosity approach to treat the phase change [24]. Thermodynamic equilibrium is assumed within each cell. Fluid flow is governed by the incompressible Navier–Stokes equation with the Boussinesq–approximation. The two–phase region is modelled after Darcy by adding a standard porous medium source term [25] after Carman–Kozeny [26]. Volume expansion during freezing has been neglected.

The SIMPLER algorithm of Patankar [23] is used to treat pressure–velocity coupling. The advection term is discretized with the Hybrid Scheme, and the transient term with Crank–Nicolson [22].

Our model is able reproduce the development of brine channels during one–dimensional ice growth if run on sufficiently fine grids (1 mm grid), reproduces an abrupt onset of convection [27], and develops a region of reduced salinity at the center if applied to crack refreezing problems (1 cm grid).

We can only outline the three key observations at this point. However, they support our assumptions on the refreezing process, and should be mentioned. The general convection pattern is, apart from occasional disturbances due to brine rejection at the ice–air interface, seawater flowing up the center, and brine flowing down at the sides. The upwelling seawater splits at the ice–air interface to form a V–shaped pattern. Convection gets weaker during the course of the refreezing process.

5. Summary and Conclusion

We have presented an account of the salinity profile, inclusion alignment, and crystal structure of two cracks that refroze in a supposed divergent regime, and of artificial cracks, or slots, that refroze under known conditions. We found that distinct features of this kind of two–dimensional growth are

© NRC Canada

arch shaped alignment of inclusions, tilted growth of crystals, and a symmetric salinity profile with a region of low salinity at the center. To better account for the observations we have described the results of numerical simulations of the crack refreezing process. These calculations confirmed that convective currents during refreezing are likely, and that seawater is generally advected upwards at the center, while salty brine is removed along the sides of the crack.

With the help of convective currents we were able to account qualitatively for our observations. The possibility of rejected brine flowing down sloped interfaces of the crack side walls could explain the observations of Niederauer and Martin [7] and others that in the early stages of brine channel development the channels tend to slope towards the cooler and thicker side. There should then be a threshold ice–water interface slope that marks the transition between brine channels inclined at an angle to the vertical, and inclusion alignment that follows the interface.

Acknowledgements

The authors wish to say thanks for their great support to Dave Hardisty, Myles Thayer, Barbara Buchanan, Peter Stroud, Dale Watts, and Dr. Colin Wells in preparation of the experiments, and in the field to Dr. Dave Cole, Dr. Jean–Louis Tison, Dave Cochrane, Simon Gibson, Eberhardt Deuss, Jonathan Leich, and Scott Base staff, and to Antarctica New Zealand.

References

1. W.F. Weeks and S.F. Ackley. CRREL Monograph 82–1, U.S. Army Cold Reg. Res. and Eng. Lab., Hanover, N.H.. 1982.
2. H. Eicken. J. Geophys. Res. **97**(C10), 15545 (1992).
3. R.A. Lake and E.L. Lewis. J. Geophys. Res. **75**(3), 583 (1970).
4. M. Nakawo and N.K. Sinha. ao **22**(2), 193 (1984).
5. N. Untersteiner. J. Geophys. Res. **73**(4), 1251 (1968).
6. K.O. Bennington. J. Glaciol. **6**(48), 845 (1967).
7. T.M. Niederauer and S. Martin. J. Geophys. Res. **84**(C3), 1176 (1979).
8. D.M. Cole and L.H. Shapiro. J. Geophys. Res. **103**(C10), 21739 (1998).
9. F. Cottier, H. Eicken, and P. Wadhams. J. Geophys. Res. **104**(C7), 15545 (1999).
10. G. Amberg and G.M. Homsy. J. Fluid Mech. **252**, 79 (1993).
11. R.C. Picu, V. Gupta, and H.J. Frost. J. Geophys. Res. **99**(B6), 11775 (1994).
12. T.P. Schulze and W.G. Worster. J. Fluid Mech. **388**, 197 (1999).
13. D.L. Feltham, M.G. Worster, and J.S. Wettlaufer. J. Geophys. Res. **107**(C2), 1–1 (2002).
14. L.I. Eide and S. Martin. J. Glaciol. **14**(70), 137 (1975).
15. G.F.N. Cox and W.F. Weeks. CRREL Res. Rep. 345, U.S. Army Cold Reg. Res. and Eng. Lab., Hanover, N.H.. 1975.
16. M. Wakatsuchi and T. Kawamura. J. Geophys. Res. **92**(C7), 7195 (1987).
17. S. Tait and C. Jaupart. J. Geophys. Res. **97**(B5), 6735 (1992).
18. J.S. Wettlaufer, M.G. Worster, and H.E. Huppert. J. Fluid Mech. **344**, 291 (1997).
19. C.F. Chen. J. Fluid Mech. **293**, 81 (1995).
20. T.G. Haskell, W.H. Robinson, and P.J. Langhorne. Cold Reg. Sci. Technol. **24**, 167 (1996).
21. J.K. Lewis, W.B. Tucker III, and P.J. Stein. J. Geophys. Res. **99**(C8), 16361 (1994).
22. H.K. Versteeg and W. Malalasekera. An introduction to computational fluid dynamics. Pearson Education Ltd., London. 1995.
23. S.V. Patankar. Numerical heat transfer and fluid flow. Hemisphere Publishing Co., New York. 1980.
24. V.R. Voller and C. Prakash. Int. J. Heat Mass Transfer **30**(8), 1709 (1987).
25. S.D. Felicelli, J.C. Heinrich, and D.R. Poirier. Metall. Trans. B **22B**, 847 (1991).
26. F. Golfier, C. Zarcone, B. Bazin, R. Lenormand, D. Lasseux, and M. Quintard. J. Fluid Mech. **457**, 213 (2002).
27. J.S. Wettlaufer, M.G. Worster, and H.E. Huppert. J. Geophys. Res. **105**(C1), 1123 (2000).

© NRC Canada